JCI insight

ADAMTS2 and ADAMTS14 substitute ADAMTS3 in adults for proVEGFC activation and lymphatic homeostasis

Laura Dupont, … , Agnès Noël, Alain CMA Colige

JCI Insight. 2022. https://doi.org/10.1172/jci.insight.151509.

Research In-Press Preview Angiogenesis Vascular biology

Graphical abstract

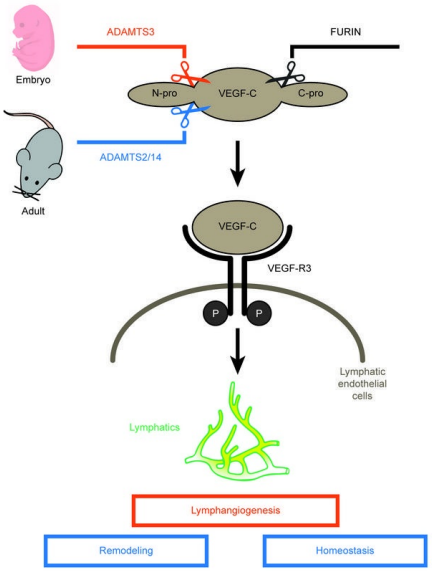

ADAMTS2 and ADAMTS14 substitute ADAMTS3 in adults for proVEGFC activation and lymphatic homeostasis.

Laura Dupont[1, 2], Loïc Joannes[2], Florent Morfoisse[1, 3], Silvia Blacher[1], Christine Monseur[2], Christophe F. Deroanne[2], Agnès Noël[1]*, Alain CMA Colige[2]*

[1]Laboratory of Tumor and Developmental Biology, GIGA-R, University of Liege, 4000 Sart Tilman, Belgium.

[2]Laboratory of Connective Tissues Biology, GIGA-R, University of Liege, 4000 Sart Tilman, Belgium.

[3]Institute of Metabolic and Cardiovascular diseases of Toulouse, INSERM UMR 1048, 31432 Toulouse, France.

*These authors contributed equally.

Corresponding author: Dupont Laura

Phone Number: +32/43669293

Address: Avenue Hippocrate n°13 B23/+3, 4000 Sart Tilman, Belgium

E-mail address: ldupont@uliege.be

Conflicts of interest:

The authors declare that no competing interests exist.

Abstract:

The capacity of ADAMTS3 to cleave proVEGFC into active VEGFC able to bind its receptors and to stimulate lymphangiogenesis has been clearly established during the embryonic life. However such function of ADAMTS3 is unlikely to persist in adulthood because of its restricted expression pattern after birth. Since ADAMTS2 and ADAMTS14 are closely related to ADAMTS3 and are mainly expressed in connective tissues where the lymphatic network extends, we hypothesized that they could substitute ADAMTS3 during adulthood in mammals for proteolytic activation of proVEGFC. Here, we demonstrated that ADAMTS2 and ADAMTS14 are able to process proVEGFC and activate the downstream pathway as efficiently as ADAMTS3. In vivo, adult mice lacking *Adamts2* develop skin lymphedema due to a reduction of the density and diameter of lymphatic vessels leading to a decrease of lymphatic functionality, while genetic ablation of *Adamts14* has no impact. In a model of thermal cauterization of cornea, lymphangiogenesis was significantly reduced in *Adamts2* and *Adamts14* knockout mice, and further repressed in *Adamts2/Adamts14* double knockout mice. In summary, we have demonstrated that ADAMTS2 and ADAMTS14 are as efficient as ADAMTS3 for proVEGFC activation and are involved in the homeostasis of the lymphatic vasculature in adulthood, both in physiological and pathological processes.

Introduction:

The lymphatic vasculature plays critical homeostatic functions such as interstitial fluid and macromolecule drainage, local coordination of immunity and immune cell trafficking (1, 2). The complete absence of lymphatic development leads to embryonic lethality, while lymphatic dysfunctions in adulthood are also implicated in several acquired pathologies such as secondary lymphedema, psoriasis and cancer. The most specific lymphatic molecular determinants have been identified through genetic studies of primary lymphatic defects in human and through the use of transgenic animal models, especially in mice and fishes (2, 3). These studies have identified the VEGFC/VEGFR3 axis as a central player in lymphangiogenesis. VEGFC is a ligand of VEGFR3, a receptor mainly expressed by lymphatic endothelial cells but also present on blood vessel endothelial cells during angiogenic processes. VEGFD is also a VEGFR3 ligand able to stimulate lymphangiogenesis, but its loss in VEGFD deficient mice and fishes does not lead to an obvious phenotype (4). VEGFC and D are both synthesized as pro-molecules requiring the cleavage of the amino- and carboxy- terminal domains to acquire the capacity to bind and activate efficiently VEGFR3 (5). The C-propeptide of VEGFC and D are both cleaved by furin and similar enzymes. However, different processes are implicated for the removal of the N-propeptides. Serine proteases are the processing enzymes for VEGFD, while ADAMTS3 cleaves the N-propeptide of proVEGFC with CCBE1 (Collagen and calcium-binding EGF domain-containing protein 1) acting as a co-factor (6, 7). Accordingly, the genetic deletion of *Ccbe1* or *Adamts3* in mouse models leads to similar phenotypes characterized by a total absence of primary lymphatic network formation, which causes embryonic lethality. In human patients, missense hypomorphic mutations in *CCBE1* or *ADAMTS3* (8-10) lead to similar primary lymphedema diseases, named Hennekam lymphangiectasia-lymphedema syndrome 1 and 3, respectively. In zebrafish, the absence of *adamts3* does not cause lymphatic defects, as seen in mammals, and only the simultaneous loss of *adamts3* and *adamts14* recapitulates the phenotype

seen in absence of *ccbe1* or *vegfc*. These findings suggest that Adamts3 and Adamts14 can display redundant functions in zebrafish embryo (11).

While the proteolytic activation of proVEGFC by ADAMTS3 is now well demonstrated during embryogenesis, it is not likely to occur in adults. Indeed, after birth, ADAMTS3 expression becomes mainly restricted to the central nervous system and the cartilage (12). On the other hand, the proteolytic activation of proVEGFC must occur in adulthood for lymphatic homeostasis, as highlighted by models in which the overexpression of proVEGFC in adult skin stimulates lymphangiogenesis (13). These observations clearly demonstrate that one or several enzymes can substitute ADAMTS3 in adults and could therefore be implicated in lymphatic regulation. ADAMTS2 and ADAMTS14 share high sequence homology and an identical domain composition with ADAMTS3 (14). ADAMTS2 is expressed by cells of mesenchymal origin (fibroblasts, smooth muscle cells, adipocytes …) while ADAMTS14 is moderately produced by several cell types, including mesenchymal cells and some immune cells. Knockout mice have been generated to investigate the in vivo functions of these three related ADAMTS. Genetic ablation of *Adamts3* leads to embryonic lethality at 15-days post coitus due to the lack of lymphatic vessels development (7), in direct relationship with the capacity of ADAMTS3 to cleave proVEGFC into active pro-lymphangiogenic VEGFC. At birth, *Adamts2*-KO pups are undistinguishable from their wild type littermates. However, within 3 weeks, their skin becomes highly fragile because of the accumulation of incompletely processed procollagen molecules forming abnormal collagen fibrils (15). This clearly illustrates the critical role of ADAMTS2 for the cleavage of the aminopropeptide of fibrillary collagens, an activity at the origin of the name “aminoprocollagen peptidase” given to the subfamily of ADAMTS formed by ADAMTS2, 3 and 14. Finally, *Adamts14*-KO do not display any obvious morphological phenotype. However, mice deficient for both *Adamts2* and *Adamts14* develop, during ageing, skin lesions reminiscent of atopic dermatitis, which are not seen in single-KO mice and suggest

dysregulation of the immune system (16). In addition to being able to cleave the amino-propeptide of fibrillar collagens, ADAMTS2, 3 and 14 can also cleave several common substrates at identical cleavage sites usually after nonpolar or slightly hydrophobic amino acids such as Pro, Gly, Ala or Val (17).

Since ADAMTS2 and 14 are mainly expressed in connective tissues where the lymphatic network extends, we reasoned that they could substitute ADAMTS3 during adulthood in mammals for proteolytic activation of proVEGFC at a site (A^{111}-^{112}A in human, A^{107}-A^{108} in mouse) fully compatible with a cleavage by ADAMTS2 and ADAMTS14. We here provide evidence that ADAMTS2 and ADAMTS14 are key actors of proVEGFC processing in adulthood.

Results

ADAMTS2/ADAMTS14 control the processing of proVEGFC and are thus required to generate its biologically active form

In mouse, ADAMTS3 is abundant in all connective tissues during embryonic development (12) explaining why, at that stage, it is the main enzyme processing proVEGFC into active VEGFC. However, its expression is reported to decrease after birth and to become restricted to brain and cartilage, while ADAMTS2 (mesenchymal cells in general, macrophages …) and ADAMTS14 (fibroblasts, granulocytes …) are more widely expressed (12) (see also "The Human Protein Atlas": https://www.proteinatlas.org and "BioGPS": http://biogps.org). We investigated their respective expressions in embryos at 12.5 and 14 days post-coitus (dpc), and in the skin of 18 dpc embryos, young pups and adult mice (Supplemental Figure 1). As expected, the expression of *Adamts3* was high in 12.5 and 14 dpc embryos, but much reduced at 18 dpc and postnatally. In sharp contrast, *Adamts2* and *Adamts14* were produced from 14 dpc and their expression remained constant, and at a higher level at later stages than *Adamts3*, suggesting that they could potentially substitute its role in lymphangiogenesis during adulthood. To investigate a potential role of ADAMTS2 and 14 in lymphangiogenesis, we first evaluated their capacity to activate proVEGFC in vitro. The conditioned medium from HEK293 cells overexpressing proVEGFC was collected and incubated with recombinant ADAMTS2, ADAMTS14 or ADAMTS3 used as a positive control (Supplemental Figure 2). When produced by HEK293 cells, VEGFC is secreted as two major forms corresponding to the full size protein (at 61 kDa) after removal of the signal peptide (at 58 kDa) and to a product (around 31 kDa) resulting from the cleavage of the C-propeptide by pro-protein convertases such as furin (Figure 1, lane 1). Upon incubation with ADAMTS3, the cleavage of the N-propeptide is illustrated by the presence of products at 45 kDa and 21 kDa (Figure 1, lane 2). The same migration pattern was observed after incubation with ADAMTS2 and ADAMTS14 demonstrating that these 2 enzymes can cleave proVEGFC

(lanes 4, 6). EDTA-induced inhibition of ADAMTS3, ADAMTS2 or ADAMTS14 completely abolished proVEGFC processing (lanes 3, 5 and 7). The localization of the cleavage site was determined and proved to occur between Ala^{111} and Ala^{112} for the three ADAMTS. Finally, a functional assay has been performed to confirm that this proteolytic processing can indeed activate proVEGFC into VEGFC. Lymphatic endothelial cells (LEC) were treated with proVEGFC-enriched medium pre-incubated with or without ADAMTS2, 3 or 14. After 5 min of treatment, cells were lysed and Western blot analysis was performed using an antibody specific for a phosphorylated form of VEGFR3, used as a readout of VEGFR3 activation by the fully processed VEGFC (Figure 2). Receptor phosphorylation was induced when proVEGFC was cleaved by ADAMTS3 (compare lane 1 to lanes 2 and 4), but not when ADAMTS3 was inhibited by the presence of EDTA (lanes 3 and 5) (Figure 2A). Most interestingly, the same levels of VEGFR3 phosphorylation were observed when ADAMTS2 (lanes 6 and 8) or ADAMTS14 (lanes 10 and 12) were used instead of ADAMTS3. Visualization of total VEGFR3 on the same blot revealed similar patterns for all the samples (Figure 2B), which confirmed that the increased signals observed when proVEGFC was incubated with active ADAMTS resulted from increased phosphorylation and not from an increased amount of VEGFR3. Similar results were observed regarding the phosphorylation of VEGFR2 (Supplemental Figure 3).

Presence of lymphedema in *Adamts*2 knockout mice

Having clearly demonstrated that ADAMTS2 and ADAMTS14 are as efficient as ADAMTS3 in vitro for activating proVEGFC, we investigated if their activity is also functionally important in vivo. We first evaluated signs of potential lymphedema by measuring the diameter of the tail base of adult mice knockout for *Adamts2* ($TS2^{-/-}$), for *Adamts14* ($TS14^{-/-}$) and for both *Adamts2* and *Adamts14* ($TS2^{-/-}TS14^{-/-}$). An increased diameter of the tail base was observed for single $TS2^{-/-}$ and double $TS2^{-/-}TS14^{-/-}$ mice, as compared to WT mice, but not for single $TS14^{-/-}$ mice

(Figure 3A). Edema was associated with histological changes showing swelling of the dermis, as illustrated by an increase of its relative proportion on tissue sections (Figure 3B) and by decrease of its eosin staining (Figure 3C). Moreover, tail skin samples were also weighed, fresh and after desiccation, showing that the water content was higher in $TS2^{-/-}$ and $TS2^{-/-}TS14^{-/-}$ (Figure 3D). Similar data were obtained when measuring edema at the level of paws (Supplemental Figure 4).

Impaired lymphatic network and function in absence of *Adamts2* and/or *Adamts14* in adult mice

In order to determine if the lymphatic network is altered in adults lacking *Adamts2* and/or *Adamts14*, whole mounts of dorsal ear skin were stained and evaluated by immunofluorescence. In this model, the structure of the lymphatic network varies according to the distance from the edge of the ear, the vessels being small, highly branched and dense at the periphery, while being less numerous and larger towards the center. This specific distribution of the ear lymphatic vasculature was taken into account by determining the spatial distribution of normalized lymphatic vessel frequency starting at the ear border. This frequency was significantly reduced in $TS2^{-/-}$ and in $TS14^{-/-}$, and even more strongly in $TS2^{-/-}TS14^{-/-}$. The analysis of the curves (Kolmogorov-Smirnov test) indicates that the spatial distributions of the lymphatic vessels are strongly affected in $TS2^{-/-}TS14^{-/-}$ mice, but also modified in $TS2^{-/-}$ and in $TS14^{-/-}$ mice as compared to WT (Figure 4A and B). In sharp contrast, no difference was seen regarding blood vessels, showing that these alterations specifically affect the lymphatic vasculature (Supplemental Figure 5). A reduced diameter of the lymphatics in $TS2^{-/-}$ and in $TS2^{-/-}TS14^{-/-}$ compared to WT and $TS14^{-/-}$ mice was also observed (Figure 4C).

As a complementary model to get an insight into potential functional consequences of these alterations, we injected Evans blue dye in the footpad of mice of the four genotypes and

evaluated its presence in inguinal lymph nodes. Thirty minutes after the injection, lymph nodes and the efferent lymphatic vessels had a marked blue color in WT and TS14$^{-/-}$ mice, while they were barely detectable in TS2$^{-/-}$ and TS2$^{-/-}$TS14$^{-/-}$ mice demonstrating a delayed draining from the site of injection and, therefore, a clear reduction of the functionality of the lymphatic network (Figure 5).

Involvement of *Adamts2* in postnatal lymphatic network homeostasis

In order to evaluate if *Adamts2* and *Adamts14* participate in the postnatal homeostasis of the lymphatic network in vivo, skin samples were collected from 6-day-old pups. In WT mice, LYVE1 staining revealed the presence of lymphatics in the upper dermis in close association with the bulge region of the hair follicle (Figure 6), as expected (18), while the LYVE1 positive cells identified in the lower dermis and in the adipose tissue were mainly macrophages (Supplemental Figure 6). The density of lymphatics was not modified in TS14$^{-/-}$, but markedly reduced in TS2$^{-/-}$ and TS2$^{-/-}$TS14$^{-/-}$ mice (Figure 6), indicating that lymphedema observed in the adulthood most probably results from early postnatal defects.

***Adamts2/Adamts14* ablation affects pathological lymphangiogenesis**

To investigate the mechanism leading to lymphatic vessel neoformation in adults, we used the model of thermal cauterization-induced corneal lymphangiogenesis which relies on VEGFC signaling and mimics lymphangiogenesis induced upon inflammatory conditions such as keratitis, chemical burns and graft rejection (19, 20). Although the cornea is an avascular tissue, it is rapidly colonized after thermal cauterization by lymphatic vessels arising perpendicularly from the limbal vascular arcade. In WT mice, *Adamts2* is expressed in control cornea, and its expression is still increased upon thermal cauterization (Figure 7A). While *Adamts3* remained poorly expressed under physiological and pathological conditions, *Adamts14* was clearly upregulated during the repair process. As compared to WT mice, a drastic reduction of neo-

lymphangiogenesis was observed in $TS2^{-/-}TS14^{-/-}$ mice in terms of vessel length, number and branching (Figure 7B, C, D and E). Interestingly, intermediate values were observed in $TS2^{-/-}$ and $TS14^{-/-}$ mice, suggesting that the two enzymes are equally involved in the process. It is worth noting that the effect of ADAMTS deficiency is restricted to the lymphatic system since corneal blood vessels network remains unaffected (Supplemental Figure 7).

Discussion

The processing of proVEGFC into VEGFC is a rate limiting step for lymphangiogenesis, since it is required to endow VEGFC with its capacity to bind and activate VEGFR3 and VEGFR2. ADAMTS3 is involved in this crucial function during embryonic lymphangiogenesis (6, 7). However, given its restricted expression pattern in adults, it is unlikely that ADAMTS3 still performs this function in adulthood.

ADAMTS3 possesses high similarity with ADAMTS2 and ADAMTS14 in terms of sequence and domain composition. These three enzymes also share the capacity to cleave the aminopropeptide of fibrillar collagens, but with different efficacy: ADAMTS2 being the most efficient, and ADAMTS3 and ADAMTS14 displaying only moderate and low activities, respectively (12, 14, 17, 21, 22). By sharp contrast, we have shown here that the three enzymes display similar processing activities when proVEGFC was used as substrate, showing that it might be a more physiological substrate for ADAMTS14 than fibrillar procollagens and, therefore, that ADAMTS14 activity could be more important for lymphangiogenesis than for collagen maturation. So far, mice knockout for *Adamts2* or *Adamts14* have been used mainly to determine their implications in collagen biology and were never specifically investigated for potential lymphatic defects. Of notes, however, mice lacking both *Adamts2* and *Adamts14* ($TS2^{-/-}TS14^{-/-}$) display a peculiar phenotype consisting in the formation of skin lesions caused by localized accumulation of inflammatory cells (16), a feature that could result from lymphatic defects since lymphatic vasculature plays a crucial role in resolving inflammation (23).

Potential existence of skin lymphedema was first evidenced by measuring the diameter of the tail base and of paw. Significant differences were found for $TS2^{-/-}$ and $TS2^{-/-}TS14^{-/-}$ mice, as compared to WT mice, which were further confirmed on histological tissue sections, by measurements of their skin water content and by evidencing a strong reduction of fluid drainage with both the inguinal lymph node and the efferent lymphatic vessel being barely stained after

Evans blue dye injection in the footpad. In order to get a better insight into the causes leading to reduced drainage, we performed ear skin whole mount staining in order to get an overview of the lymphatic network. As compared to WT mice, we found a reduction of the density of lymphatic vessels in $TS2^{-/-}$ and $TS14^{-/-}$ mice which was even more pronounced in $TS2^{-/-}TS14^{-/-}$ mice. This clearly indicates that both enzymes are involved and can partially compensate for each other in single KO mice. In addition, in absence of *Adamts2* ($TS2^{-/-}$ and $TS2^{-/-}TS14^{-/-}$) vessels seem to have a smaller diameter, being shrunk or less swollen, as compared to WT and $TS14^{-/-}$ mice. These data suggest that edema found in $TS2^{-/-}$ and $TS2^{-/-}TS14^{-/-}$ mice are caused by decreased functionality of the lymphatic vessels and that their slightly reduced density and branching in $TS14^{-/-}$ mice is not sufficient to induce edema in physiological conditions. The skin of 6-day-old pups was also analyzed in order to determine if alteration of the lymphatic network progressively takes place in the adulthood or very early after delivery. For technical reasons related to the size and the fragility of samples, these analyses were performed on histological cross-sections of back skin. Skin lymphatics do not have specific orientations and, as a result, their surfaces on histological sections vary strongly according to their local orientation. Therefore, we quantified the number of LYVE1 stained structures per surface of dermis and not the surface they covered, so that lymphatics in cross section or longitudinal section have the same value. Only the absence of *Adamts2* had an impact on lymphatic density, which could be attributed to the residual presence of *Adamts3* a few days after birth and to the fact that *Adamts2* is much more expressed than *Adamts14* around birth.

Having shown the impact of *Adamts2* on lymphatics in physiological conditions, we then used a model of acute neo-lymphangiogenesis occurring after injury. In the eye, lymphatic vessels are found in the conjunctiva and the limbus, in which lymphatic vasculature is a ring shaped network with very small extensions directed toward the central avascular cornea (24). However, upon inflammatory stimuli, blood and lymphatic vessels rapidly extend from the limbus

towards the cornea. The major advantage of the corneal neovascularization assay is that any vessel that grows into the corneal stroma is newly formed and can easily be detected, allowing the determination of several relevant parameters such as vessel length, invasion distance or vascular density (24). In the absence of *Adamts2* or *Adamts14*, a significant reduction of cornea invasion was observed, with lymphatics being shorter, less numerous and less branched, as compared to WT mice. Remarkably, these alterations are more obvious in $TS2^{-/-}TS14^{-/-}$ mice, demonstrating that both enzymes actively participate to lymphangiogenesis during tissue inflammation and repair. Of notes also, angiogenesis was not affected, arguing for the involvement of the VEGFC/VEGFR3 pathway since VEGFC is required for lymphangiogenesis but outcompeted by VEGFA for stimulating angiogenesis.

It was known that ADAMTS3 is required for embryonic lymphangiogenesis by its capacity to process proVEGFC into active VEGFC. Here, we have demonstrated that ADAMTS2 and ADAMTS14 are as efficient as ADAMTS3 for processing proVEGFC into active VEGFC, and that their absence in mouse models in vivo lead to alterations of the lymphatic network in adulthood.

These data open new research avenues which are beyond the scope of the present study. As a first example, it is not clear yet if CCBE1 promotes the activity of ADAMTS2 and ADAMTS14 as reported for ADAMTS3 (6). The absence of ADAMTS2 or ADAMTS14 does not involve massive edema in our mouse models, suggesting that mutations in these genes should not be responsible for primary lymphedema. However, some reduction of their activity could be part of the numerous factors increasing the sensitivity to secondary lymphedema occurring after diverse types of injuries or trauma. This hypothesis is supported by our data showing that neo-lymphangiogenesis observed in repairing cornea is almost completely prevented in absence of both ADAMTS2 and ADAMTS14. Efforts are being made now to develop inhibitors for specific ADAMTS, notably for ADAMTS5 in order to find a medication able to limit cartilage

degradation (25). Similar strategies could be used for ADAMTS2, 3 and 14 by focusing on their identical catalytic domain or on their ancillary domains allowing their interactions with their substrates. If such inhibitors are obtained, they could help to fight conditions in which excessive or abnormal lymphangiogenesis is part of the pathological mechanisms like, for example, tumor aggressiveness and the formation of premetastatic niches in the lymph nodes.

Materials and methods

Transgenic mice

Wild-type (WT), *Adamts14*$^{-/-}$, *Adamts2*$^{-/-}$ and *Adamts2*$^{-/-}$/*Adamts14*$^{-/-}$ C57bl/6 mice were used throughout this study, either at postnatal day 6 or at 8 to 10-week-old (see references 15 and 16 for initial descriptions). The animals were maintained under a 12-h light-dark cycle with free access to food and water. Animal experiments were performed in compliance with the Animal Ethical rules of the University of Liège (Liège, Belgium) after approval of the local Animal Ethical Committee.

RT-PCR

The different tissues were dissected and snap-frozen. RNA was isolated using the Nucleospin RNA/protein extraction kit (Macherey Nagel, 740933.50). RT-PCR amplifications were performed using Tth DNA Polymerase (Roche, Bâle, Switzerland). RT-PCR products were observed after electrophoresis in acrylamide gels and staining with Gel Star (50535, Lonza). The following primers and cycles were used: 5′-CAGGCG CACACATAGTACCATCCA-3′ (reverse primer, sequence corresponding to exon 10) and 5′-CAGCCGCTACCTGCATTCCTATGA-3′ (forward primer, junction of exons 8 and 9) for *Adamts2* (28 cycles); 5′-GATACATCTCTGGGAGGCTGCTCCA-3′ (reverse primer, exon 22) and 5′-GCTGTGCCTATGTTGGTGACATCA-3′ (forward primer, junction of exons 20 and 21) for *Adamts3* (30 cycles); 5′-CCATCCTCGTGGTTGAGGGCACA-3′ (reverse primer, exon 7) and 5′-CTGATCATGGTGGGCTACCGACA-3′ (forward primer, exon 5) for *Adamts14* (30 cycles); and 5′-GATTCTGACTTAGAGGCGTTCAGT-3′ (reverse primer) and 5′-GTTCACCCACTAATAGGGAACGTGA-3′ (forward primer) for *28S* (internal control) (16 cycles). Due to the localizations of the target sequences of the primers, only a single product

was amplified by qRT-PCR for each Adamts (at 257 bp for *Adamts2*, at 155 bp for *Adamts3* and at 236 bp for *Adamts14*).

Protein purification and VEGFC processing assay

Recombinant ADAMTS2, ADAMTS3 and ADAMTS14 were purified as previously described (26). Stably transfected cells were grown in DMEM supplemented with 10% fetal calf serum. Upon confluence, the growth medium was replaced by serum free DMEM containing soybean trypsin inhibitor (40 μg/ml), heparin (5 μg/ml), and ZnCl2 (80 μM). After 48 h the medium was collected and the recombinant ADAMTS were purified through affinity chromatography (ConA-Sepharose followed Heparin-Sepharose). Note that this method leads to the purification of several ADAMTS polypeptides with different molecular weights (26 and Supplemental Figure 2) and different activities. In order to circumvent this problem, quantifications of recombinant ADAMTS were made after SDS-PAGE and staining with SYPRO Ruby using known concentrations of BSA as reference. Only the product around 100 kDa was taken into account, since this polypeptide corresponds to the expected molecular weight of the fully mature and most active form of ADAMTS2, 3 and 14. Concentrations of enzymes were adjusted around 10 ng per μl.

HEK293 cells (Invitrogen) expressing human proVEGFC were cultured for 48 h in DMEM containing 0.1% FBS and 50 μM Decanoyl-RVKR-CMK (furin inhibitor). For the processing assay, 20 μl of conditioned medium were supplemented with NaCl (0.3M final concentration) and 8 μl of either ADAMTS2, ADAMTS3, ADAMTS14 or control buffer, in the absence or presence of 25mM EDTA (used as an inhibitor of metalloproteinases) in a total volume of 40 μl. After 18 h incubation at 37 °C, samples were denatured in reducing conditions (1x Laemmli sample buffer containing 200mM DTT). Western blotting analyses were performed using a polyclonal goat anti-human VEGFC primary antibody (1:250, R&D, AF752). Note that the

VEGFC antibody does not react with the 29 kDa C-terminal domain of VEGFC and shows relatively low affinity for the fully processed mature 21 kDa form.

Determination of the cleavage site in proVEGFC by ADAMTS2, 3 and 14

HEK293 cells expressing human proVEGFC in a doxycycline dependent manner were cultured for 60 h in serum-free DMEM containing 1% non-essential amino acids (Biowest). The conditioned medium containing proVEGFC was collected with 0.1mM AEBSF and concentrated on a 3kDa cut-off filter (Amicon Ultra-15, PLBC, membrane Ultracel-PL, 3 kD, Millipore). Total protein content was quantified (Micro BCA kit, Thermofisher) and 60µg of proteins were incubated with control buffer or with ADAMTS2, 3 or 14 for 18h at 37°C in 50 mM Tris-HCl, pH 8.0, containing 2mM $CaCl_2$ and 0.6M NaCl.

Samples were denatured in 4M guanidine HCl and labelled with different ITRAQ labels (iTRAQ Reagents Multiplex Kit, Sciex) according to manufacturer instructions. Proteins were reduced with 1mM TCEP and alkylated with 5mM iodoacetamide. Amonium Bicarbonate buffer (pH8) was added to reach 25mM before methanol acetone precipitation. The protein pellets were dissolved in NaOH and the protein quantification was performed with Nanodrop. The different protein samples were precipitated using 2D clean-up kit according manufacturer's instructions. Samples were resolubilized in ammonium bicarbonate and digested using Multi-Enzymatic Limited Digestion (MELD) as previously described (27). The LC-MS/SM analyses were performed on an Acquity M-Class UPLC (Waters) hyphenated to a Q Exactive Plus (Thermo Scientific), in nanoelectrospray positive ion mode. The trap column is a Symmetry C18 5µm (180 µm x 20 mm) and analytical column is a HSS T3 C18 1.8 µm (75 µm x 250 mm) (Waters, Corp., Milford, USA). The samples were loaded at 20 µL/min on the trap column in 98% solvent A during 3 minutes and subsequently separated on the analytical column at a flow rate of 600 nL/min with the following linear gradient: initial conditions 98% A; 5 min 93% A; 60 min 70% A; 70 min 60% A, 73 min 15% A maintained for 5min then column is reconditioned

in initial conditions. Solvent A is 0.1% formic acid in water and solvent B is 0.1% formic acid in acetonitrile. The total run time is 60 min. The mass spectrometer method is a TopN-MSMS method where N was set to 15, meaning that the spectrometer acquires one Full MS spectrum, selects the 12 most intense peaks in this spectrum (singly charged and unassigned charge precursors excluded) and makes a Full MS2 spectrum of each of these 12 compounds. The parameters for MS spectrum acquisition are: mass range from 400 to 2000 m/z; Resolution of 70,000; AGC target of 1e6 or Maximum injection time of 250 ms. The parameters for MS2 spectrum acquisition are: Isolation Window of 2.0 m/z; Normalized Collision energy (NCE) of 30; Resolution of 17,500; AGC target of 2e5 or Maximum injection time of 120 ms and a fixed first mass set at 100 m/z. The main parameters for Q Exactive Plus tune were: spray voltage of 2.3 kV, capillary temperature of 270°C and S-Lens RF level of 50.0." Data processing was performed by PEAKS X (BSI Bioinformatics Solutions). Relative quantitation was performed at the peptide level by considering the area under the curve of the corresponding extracted ion chromatograms.

Activation of VEGFC pathway

Primary human LECs (HMVEC-dLy from Lonza (CC-2810)) were cultured in EGM2-MV medium in 6-well plate until confluence. HEK293 cells expressing human proVEGFC were cultured for 48 h in DMEM containing 0.1% FBS. Conditioned medium (70 µl) was supplemented with NaCl (0.3M final concentration) and 28 µl of either ADAMTS2, ADAMTS3, ADAMTS14 or control buffer in the absence or presence of 25mM EDTA (used as an inhibitor of metalloproteinases) in a total volume of 140 µl. After 18 h incubation at 37°C, 20µL or 100µL of the incubation mixes were added to 1ml of serum-free EBM-2 medium (CC-3156, Lonza). LEC culture media were then replaced by the different digestion mixes. After 5 min, LECs were then lysed with cell lysis buffer 1× (9803, Cell Signaling) containing phosphatase and protease inhibitors (Complete and phosSTOP, Roche). Equivalent amounts of

proteins were separated on polyacrylamide gels (7,5%) and transferred onto PVDF membranes. Membranes were then blocked, incubated overnight at 4 °C with a pVEGFR3 (CY1115 Cell application) or a pVEGFR2 specific antibody (Tyr1175, #2478, Cell Signaling), washed extensively and incubated for 1 h incubation at room temperature with horseradish peroxidase-coupled secondary antibody (P0217, Dako). After washing, the peroxidase activity was revealed with an enhanced chemiluminescence assay (ECLTM Prime Western Blotting System, Sigma Aldrich) in an ImageQuantTM LAS 4000 (GE Healthcare). The membranes were then stripped, incubated with antibodies against, respectively, total VEGFR3 (MAB3757 Merck Millipore) or total VEGFR2 (#2479 Cell Signalling) and revealed as described above.

Hind limb and tail thickness measurement

Pictures of hind limb and tail base from 8-week-old mice were acquired with a camera-equipped dissection microscope (Optika). The hind limb thickness was measured using the ImageJ software, just upfront of the first footpad and the tail diameter was measured at the tail base.

Wet-to-dry weight ratio

Tail skins were removed and weighed (wet weight), and then dried for 72 h in an oven at 60°C and weighed again (dry weight). These measurements were used to determine the water content in the skin.

Immunohistological analyses

Tissues were fixed in a 4 % paraformaldehyde (PFA) solution (and eventually decalcified in EDTA 0.5M, pH8, for 3 weeks in the case of hind limb and tail base samples) and paraffin-embedded. Tissue sections (5 µm) were deparaffined, rehydrated and stained with hematoxylin/eosin for general histological examination. The percentage of dermis area in hind limb and tail was quantified using ImageJ software as a percentage of the total tissue area.

For immunofluorescence, sections were treated (Antigen retrieval, with Target retrieval solution, Dako) and then blocked with Universal blocking Reagent (HK085-5K BioGenex). Goat anti LYVE1 antibody (1/100, AF2125, R&D Systems) and/or rat anti CD31 antibody (1/150, DIA-310, Dianova) and/or rat anti F4/80 antibody (1/100, Ab16911, Abcam) were incubated overnight at 4°C. After washes with PBS, Alexa Fluor 488-coupled rabbit anti-goat antibody (1/200; A21222, Invitrogen) was incubated at room temperature for 1h. After washes with PBS, Alexa Fluor 546-coupled goat anti-rat antibody (1/200; A11081, Invitrogen) was incubated at room temperature for 1h. Slides were then washed with PBS and mounted using Dako fluorescent mounting medium (Dako). Slides were scanned using a Nanozoomer 2.0 scanner (Hamamatsu) and visualized using NDPviewer (Hamamatsu). Count of dermal lymphatic and dermal blood vessels per surface was quantified using ImageJ software.

Staining of lymphatic vessels on whole mount ear skins from adult mice

Ears from 8 to 10-week-old mice were collected and fixed in 4% paraformaldehyde overnight at 4°C. For each ear, the dorsal skin was separated from the rest of the tissue (central cartilage and the adhering ventral skin). Whole dorsal ear skins were fixed in methanol for 1h at -20°C and then blocked with 3% milk, 0,2% Triton X-100 for 1 h at room temperature. They were then incubated with a polyclonal goat anti LYVE1 antibody (1/200; AF2125, R&D Systems) and rat anti CD31 antibody (1/150, DIA-310, Dianova) overnight at room temperature. After washing in PBS, an Alexa Fluor 488-coupled rabbit anti-goat antibody (1/200; A21222, Invitrogen) was added for 2 h at room temperature. After washes with PBS, Alexa Fluor 546-coupled goat anti rat antibody (1/200; A11081, Invitrogen) were incubated at room temperature for 2h. Slides were then washed with PBS and mounted using Dako fluorescent mounting medium (Dako). Slides were scanned using a Nanozoomer 2.0 scanner (Hamamatsu) and visualized using NDPviewer (Hamamatsu). The lymphatic vessels frequency, density and thickness were quantified using ImageJ software.

Functional analysis of the lymphatic network in vivo

To evaluate lymphatic drainage, 30µL of a 3% solution of Evans blue dye (Sigma) in PBS were injected into the footpads of anesthetized mouse hind limbs. Thirty minutes after injection, mice were sacrificed and dissected to expose the inguinal lymph node. The images were acquired with a camera-equipped dissection microscope (Optika). The blue dye intensity was measured using ImageJ software. Results are expressed as percentage of WT control.

In vivo lymphangiogenesis

Thermal cauterization was induced on the cornea of 8 to 10-week-old mice. After 7 days, corneas were dissected and whole mounted for immunostaining as previously described (28-30) or snap-frozen for RNA extraction. To visualize lymphatic and blood vessels, corneas were fixed in methanol at -20°C for 1 h and then blocked with 3% milk for 1 h at room temperature. Corneas were then incubated overnight at room temperature with a polyclonal goat anti-mouse LYVE1 antibody (1/200; AF2125, R&D Systems) and with a monoclonal rat anti mouse CD31 (1/200; 553370 BD Biosciences). After washing in PBS, an Alexa Fluor 488-coupled rabbit anti-goat antibody (1/200; A21222, Invitrogen) was added for 2 h at room temperature. After washing in PBS, an Alexa Fluor 546-coupled goat anti-rat antibody (1/200; A-11081, Thermo Fisher Scientific) was added for 2 h at room temperature. After washing, the slides were scanned using a Nanozoomer 2.0 scanner (Hamamatsu) and visualized using NDPviewer (Hamamatsu). The lymphangiogenic responses were analyzed using a described computerized method (28, 31). All the results were normalized to the total cornea area and are expressed as percentage of WT control.

Statistics

Results were illustrated with GraphPad Prism 8.0 and were expressed as medians with interquartile range of different experiments. The statistical analyses were carried out with

SigmaPlot 14.0 software by using the non-parametric Kruskal-Wallis test to test whether measurements performed on the four genotypes of mice have the same distribution or not. When tests revealed differences, post-hoc Holm-Sidak test was conducted to determine which groups are different from others. The Kolmogorov-Smirnov test was used to compare the shapes of the distribution curves, and the significance levels were adjusted with Bonferroni correction for multiple comparisons.

P values are shown in figures as $*P < 0.05$, $**P < 0.01$, $***P < 0.001$. The experiments were not randomized. No blinding was done for the analysis and quantifications.

Study approval

All animal experiments were conducted at the GIGA Animal Facility of the University of Liège (ULiège; Belgium) in accordance with the Federation of European Laboratory Animal Science Associations and the local ethical committee at ULiège (approval number: 1964 and 2151).

Author contributions

LD designed, performed, and analyzed experiments, and wrote the manuscript. LJ contributed to the analyses of proVEGFC activation and to the determination of the cleavage site in proVEGFC by ADAMTS2, 3 and 14. FM designed, performed, and analyzed experiments. SB performed all computerized quantification. MC contributed to immunostaining and mice breeding. CD participated in experimental design and data interpretation. AN funded and supervised the project and ACC supervised, funded, designed the project, interpreted the data, and wrote the manuscript.

Acknowledgments

We thank all laboratory members for useful technical advice. We thank GIGA Animal Facility platforms of ULiège for technical support and mouse housing. We thank GIGA Proteomic Facility and more especially Gabriel Mazzucchelli for the technical support to determine the cleavage site in proVEGFC by ADAMTS2, 3 and 14. ACC is "Senior Research Associate" of the FRS-FNRS and LD is supported by a "FNRS" grant (FC96394). This work was supported by grants from the Fonds de la Recherche Scientifique - FRS-FNRS (FRSM, T.0183.13, PDR), the Fondation contre le Cancer (foundation of public interest, Belgium), the Fonds spéciaux de la Recherche (University of Liège), the Fondation Hospitalo-Universitaire Léon Fredericq (FHULF, University of Liège), the Walloon Region through the FRFS-WELBIO strategic research programme, the Wallonia-Brussels Federation (grant for Concerted Research Actions, A.R.C. 19/23-21 "INovLYMPHATIC").

References

1. Petrova TV, Koh GY. Biological functions of lymphatic vessels. *Science*. 2020;10;369(6500):eaax4063.
2. Alitalo K. The lymphatic vasculature in disease. *Nat Med.* 2011;17(11):1371-80.
3. Brouillard P, et al. Genetics of lymphatic anomalies. J *Clin Invest.* 2014;124(3):898-904.
4. Baldwin ME, et al. Vascular endothelial growth factor D is dispensable for development of the lymphatic system. *Mol Cell Biol.* 2005;25(6):2441-2449.
5. Künnapuu J, et al. Proteolytic Cleavages in the VEGF Family: Generating Diversity among Angiogenic VEGFs, Essential for the Activation of Lymphangiogenic VEGFs. *Biology.* 2021;10(2):167.
6. Jeltsch M, et al. CCBE1 enhances lymphangiogenesis via A disintegrin and metalloprotease with thrombospondin motifs-3-mediated vascular endothelial growth factor-C activation. *Circulation*. 2014;129(19):1962-71.
7. Janssen L, et al. ADAMTS3 activity is mandatory for embryonic lymphangiogenesis and regulates placental angiogenesis. *Angiogenesis.* 2016;19(1):53-65.
8. Alders M, et al. Mutations in CCBE1 cause generalized lymph vessel dysplasia in humans. *Nat Genet.* 2009;41(12):1272-4.
9. Brouillard P, et al. Loss of ADAMTS3 activity causes Hennekam lymphangiectasia-lymphedema syndrome 3. *Hum Mol Genet.* 2017;26(21):4095-4104.
10. Scheuerle AE, et al. An additional case of Hennekam lymphangiectasia-lymphedema syndrome caused by loss-of-function mutation in ADAMTS3. *Am J Med Genet A.* 2018;176(12):2858-2861.

11. Wang G, et al. Specific fibroblast subpopulations and neuronal structures provide local sources of Vegfc-processing components during zebrafish lymphangiogenesis. *Nat Commun.* 2020;11(1):2724.

12. Le Goff C, et al. Regulation of procollagen amino-propeptide processing during mouse embryogenesis by specialization of homologous ADAMTS proteases: insights on collagen biosynthesis and dermatosparaxis. *Development.* 2006;133(8):1587-96.

13. Jeltsch M, et al. Hyperplasia of lymphatic vessels in VEGF-C transgenic mice. *Science.* 1997;276(5317):1423-5.

14. Colige A, et al. Cloning and characterization of ADAMTS-14, a novel ADAMTS displaying high homology with ADAMTS-2 and ADAMTS-3. *J Biol Chem*. 2002;277(8):5756-66.

15. Li SW, et al. Transgenic mice with inactive alleles for procollagen N-proteinase (ADAMTS-2) develop fragile skin and male sterility. *Biochem J*. 2001 Apr 15;355(Pt 2):271-8.

16. Dupont L, et al. Spontaneous atopic dermatitis due to immune dysregulation in mice lacking Adamts2 and 14. *Matrix Biol.*, 2018;70, 140-157.

17. Bekhouche M, et al. Determination of the substrate repertoire of ADAMTS2, 3, and 14 significantly broadens their functions and identifies extracellular matrix organization and TGF-β signaling as primary targets. *FASEB J.* 2016;30(5):1741-56.

18. Peña-Jimenez D, et al. Lymphatic vessels interact dynamically with the hair follicle stem cell niche during skin regeneration in vivo. *EMBO J.* 2019;38(19):e101688.

19. Cursiefen C, et al. Time course of angiogenesis and lymphangiogenesis after brief corneal inflammation. *Cornea* 2006;25:443-447.

20. Regenfuss B, et al. Corneal (lymph)angiogenesis – from bedside to bench and back: a tribute to Judah Folkman. *Lymphat Res Biol* 2008;6:191-201.

21. Bekhouche M, Colige A. The procollagen N-proteinases ADAMTS2, 3 and 14 in pathophysiology. *Matrix Biol.* 2015;44-46:46-53.

22. Leduc C, et al. In vivo N-terminomics highlights novel functions of ADAMTS2 and ADAMTS14 in skin collagen matrix building. *Front Mol Biosci*. 2021;8:643178.

23. Schwager S, Detmar M. Inflammation and Lymphatic Function. *Front Immunol.* 2019;10:308.

24. Hos D, et al. Antilymphangiogenic therapy to promote transplant survival and to reduce cancer metastasis: what can we learn from the eye? *Semin Cell Dev Biol.* 2015;38:117-30.

25. Santamaria S. ADAMTS-5: A difficult teenager turning 20. *Int J Exp Pathol.* 2020;101(1-2):4-20.

26. Colige A, et al. Domains and maturation processes that regulate the activity of ADAMTS-2, a metalloproteinase cleaving the aminopropeptide of fibrillar procollagens types I-III and V. *J. Biol. Chem.* 2005;280, 34397–34408.

27. Morsa D, et al. Multi-Enzymatic Limited Digestion: The Next-Generation Sequencing for Proteomics? *J Proteome Res.* 2019; 18(6), 2501–2513.

28. Blacher S, et al. Additional parameters for the morphometry of angiogenesis and lymphangiogenesis in corneal flat mounts. *Exp Eye Res.* 2009;89(2):274-6.

29. Detry B, et al. Digging deeper into lymphatic vessel formation in vitro and in vivo. *BMC Cell Biol.* 2011;12, 29.

30. Detry B, et al. Matrix metalloproteinase-2 governs lymphatic vessel formation as an interstitial collagenase. *Blood*. 2012;119, 5048–5056.

31. Detry B, et al. Sunitinib inhibits inflammatory corneal lymphangiogenesis. *Invest. Ophthalmol. Vis. Sci.*2013 54, 3082–3093.

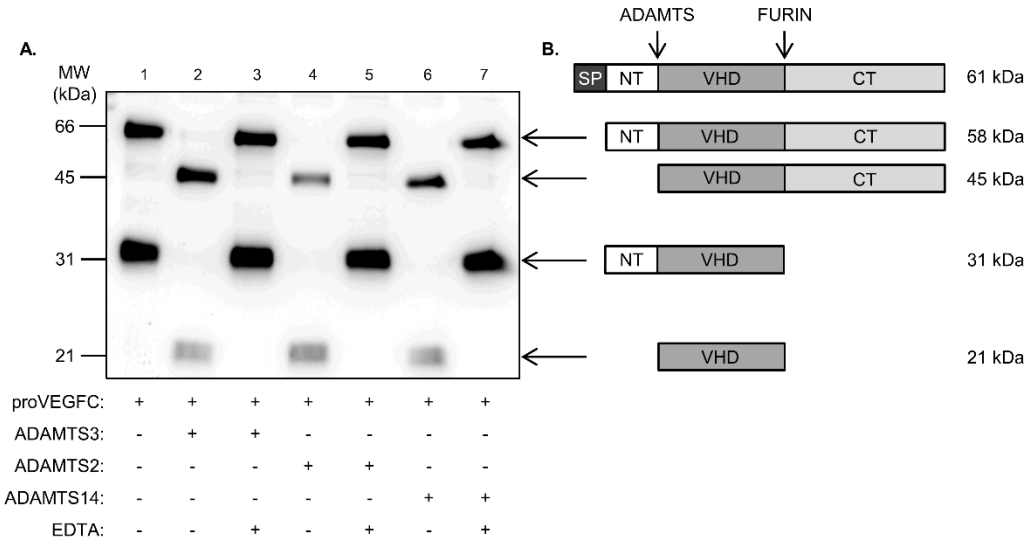

Figure 1: Processing of human proVEGFC by ADAMTS3, ADAMTS2 and ADAMTS14 proteases.

A. Conditioned medium from HEK293 cells expressing full-length proVEGFC was incubated with buffer (as negative control, lane1), ADAMTS3 (as positive control), ADAMTS2 or ADAMTS14, in the presence or absence of EDTA used as inhibitor. The electrophoretic pattern of VEGFC was analyzed by western blotting in reducing conditions. In absence of active enzymes (lane 1, 3, 5 and 7), VEGFC can be detected as a 58 kDa (full length proVEGFC without signal peptide) and a 31 kDa form generated by C-terminal processing by furin. In the presence of active ADAMTS3 (lane 2), ADAMTS2 (lane 4) and ADAMTS14 (lane 6), the 58 kDa form is totally converted into a 45 kDa polypeptide while the 31 kDa form is processed into the fully mature 21 kDa VEGFC, which is in line with N-terminal processing of VEGFC proteins.

B. Schematic illustration of the different VEGFC forms and their molecular weight is provided on the right part of the panel (SP: signal peptide; NT: N-terminal propeptide; VHD: VEGF homology domain; CT; C-terminal propeptide).

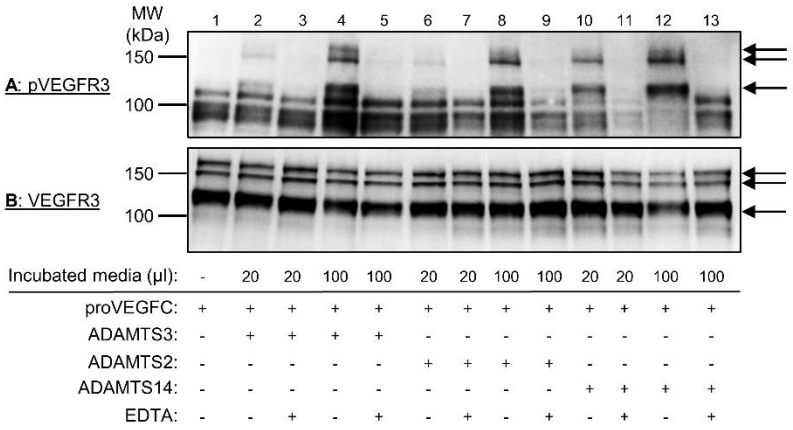

Figure 2: Phosphorylation of VEGFR3 by proVEGFC activated or not by ADAMTS3, ADAMTS2 or ADAMTS14.

Conditioned medium from HEK293 cells expressing full-length proVEGFC was first incubated for 18 hours with buffer alone (lane 1, negative control), ADAMTS3 (as positive control), ADAMTS2 or ADAMTS14, in the presence or absence of EDTA used as inhibitor. These different pretreated media were then added (20 µL or 100 µL) into 1 ml of serum-free EBM-2 on LECs cultures. After 5 min, cells were lysed, and phosphorylated VEGFR3 (A: pVEGFR3) was visualized by western blotting. After stripping of the antibodies, the same membrane was then used to visualize total VEGFR3 (B). Treatment of the proVEGFC-rich conditioned medium with active ADAMTS3, ADAMTS2 and ADAMTS14 induced the phosphorylation of the three bands corresponding to VEGFR3 (arrows on the right part of the panels) in a dose dependent manner, while the total amount of VEGFR3 was not affected, demonstrating that the processing of proVEGFC by ADAMTS2, ADAMTS3 or ADAMTS14 similarly leads to its activation.

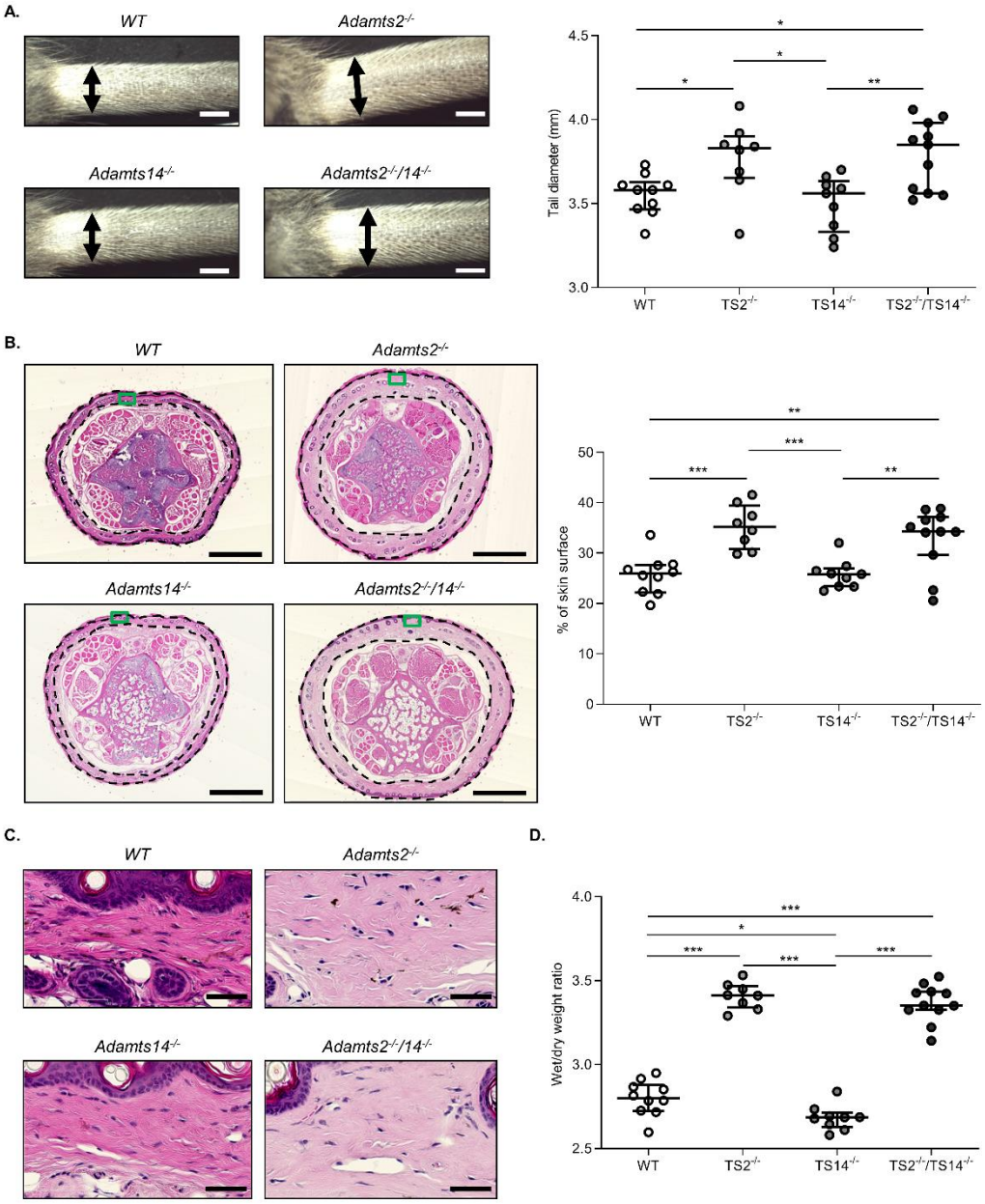

Figure 3: Tail swelling in absence of *Adamts2*.

A. Representative pictures of tails from 8-week-old WT, TS2$^{-/-}$, TS14$^{-/-}$ and TS2$^{-/-}$TS14$^{-/-}$ mice. The base tail diameters were measured (double arrows on pictures) (scale bar: 2mm). As compared to WT, the diameters are increased in TS2$^{-/-}$ and in TS2$^{-/-}$TS14$^{-/-}$ mice suggesting potential lymphedema. B. Hematoxylin-eosin staining on paraffin-embedded sections of tails were performed to further characterize which tissue compartment is responsible for the increased diameter (scale bar: 1 mm). For each section of each genotype, the percentage of surface covered by the dermis (delimited by black dotted lines) was determined (ImageJ software) and was found to be increased in TS2$^{-/-}$ and TS2$^{-/-}$TS14$^{-/-}$ mice. C. Higher magnification (scale bar: 50µm) of parts of the pictures in B (corresponding to the green boxes) showing a dermis less stained, because swollen and less dense, in TS2$^{-/-}$ and TS2$^{-/-}$TS14$^{-/-}$ mice. D. Tail skins were removed and weighed (wet weight), and then dried for 72 h in an oven at 60°C before to be reweighed (dry weight) to determine the ratios of wet to dry weight. An increase of water content was confirmed in TS2$^{-/-}$ and TS2$^{-/-}$TS14$^{-/-}$ mice. Statistical analyses were performed using Kruskal-Wallis test followed by Holm-Sidak post hoc test for multiple comparisons. $*P < 0.05$; $**P < 0.01$; $***P < 0.001$.

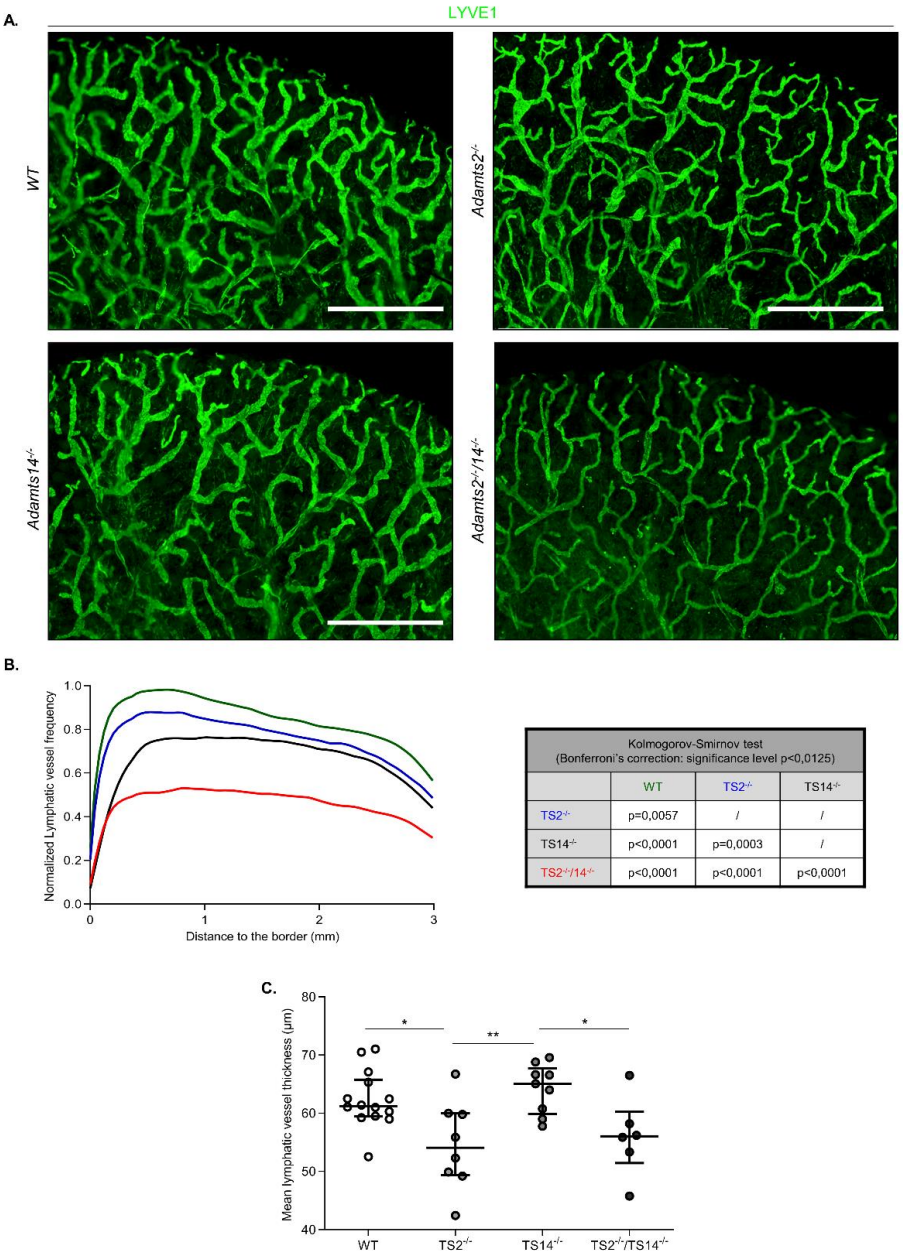

Figure 4: Absence of *Adamts2* and/or *Adamts14* affects the lymphatic network under physiological conditions in adult mice.

A. Whole mounts of dorsal ear skin were stained with an antibody specific of LYVE1 for immunofluorescence visualization of lymphatics (scale bar: 1mm). B. For computerized quantification, lymphatic vessel frequencies were determined according to the distance from the border of the ear because the structure and density of the lymphatic network vary according to the distance from the ear edge. The shape of the distribution curves were found to be statistically different ("Kolmogorov-Smirnov" test, significance levels were adjusted with Bonferroni correction for multi-comparison, see the accompanying table). The most dramatic reduction was observed in $TS2^{-/-}TS14^{-/-}$ mice, but it was also found to be reduced in $TS2^{-/-}$ and in $TS14^{-/-}$ mice as compared to WT. By sharp contrast, no difference was seen regarding blood vessels, showing that these alterations affect specifically lymphatics (Supplemental Figure 5). C. Computerized quantifications of mean diameter of the lymphatic vessels were also performed and demonstrated a smaller diameter in $TS2^{-/-}$ and $TS2^{-/-}TS14^{-/-}$ mice. Statistical analyses were performed using Kruskal-Wallis test followed by Holm-Sidak post hoc test for multiple comparisons. $*P < 0.05$, $**P < 0.01$.

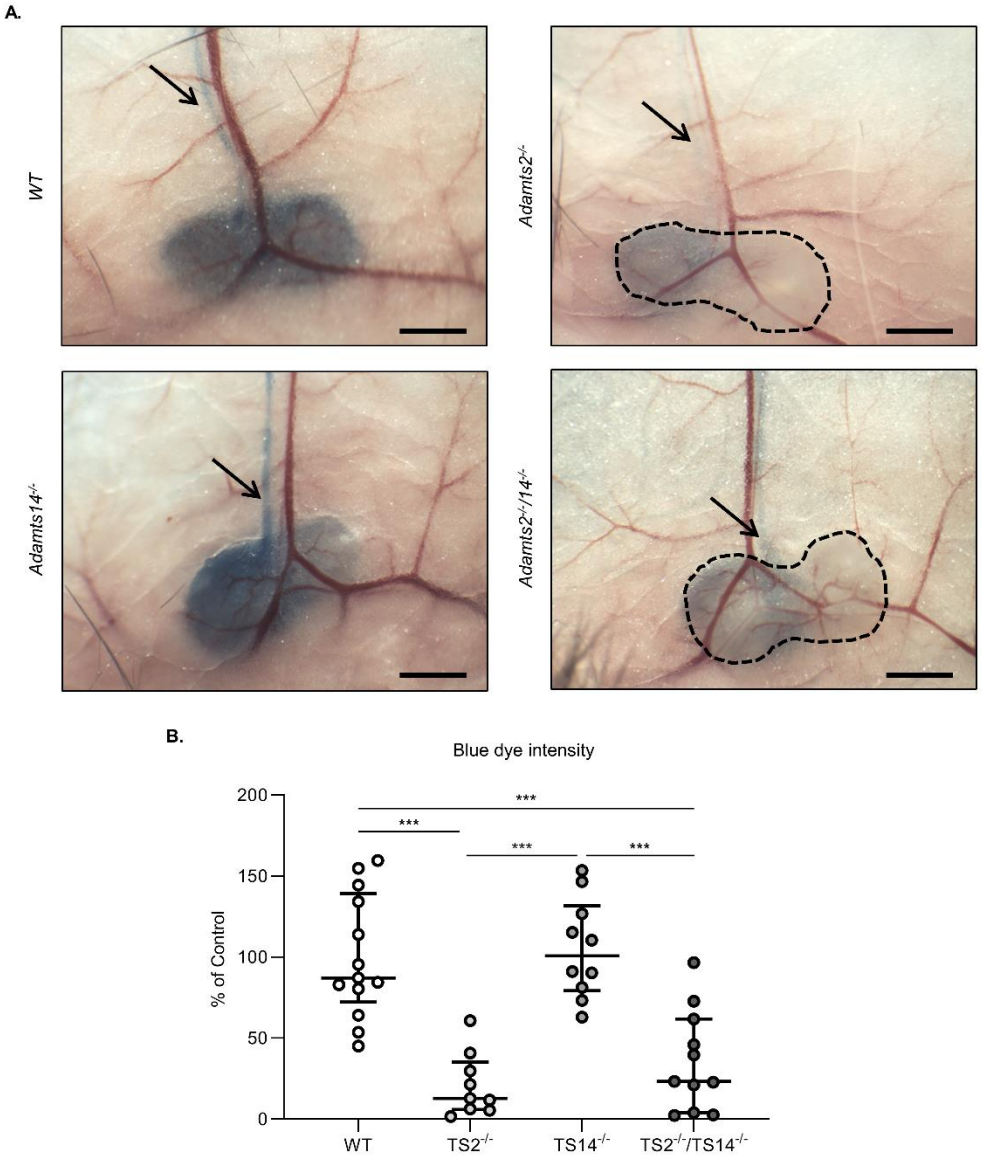

Figure 5: Impaired lymphatic function in absence of *Adamts2*.
A. Evans blue dye was injected into the footpad. After 30 min, mice were sacrificed and inguinal lymph nodes were visualized (scale bar: 1mm). In WT and TS14$^{-/-}$ mice, lymph nodes and the efferent lymphatic vessels (arrows) had a marked blue color. By contrast, they were barely detectable in TS2$^{-/-}$ and TS2$^{-/-}$TS14$^{-/-}$ mice demonstrating a delayed draining from the site of injection. The images were acquired with a camera-equipped dissection microscope (Optika). B. Computer-assisted quantification of the blue dye intensity in inguinal lymph node of WT, TS2$^{-/-}$, TS14$^{-/-}$ and TS2$^{-/-}$TS14$^{-/-}$ mice are expressed as percentage of WT control. Outliers were excluded based on Dixon's test for extreme values. Statistical analyses were performed using Kruskal-Wallis test followed by Holm-Sidak post hoc test for multiple comparisons. $***P < 0.001$.

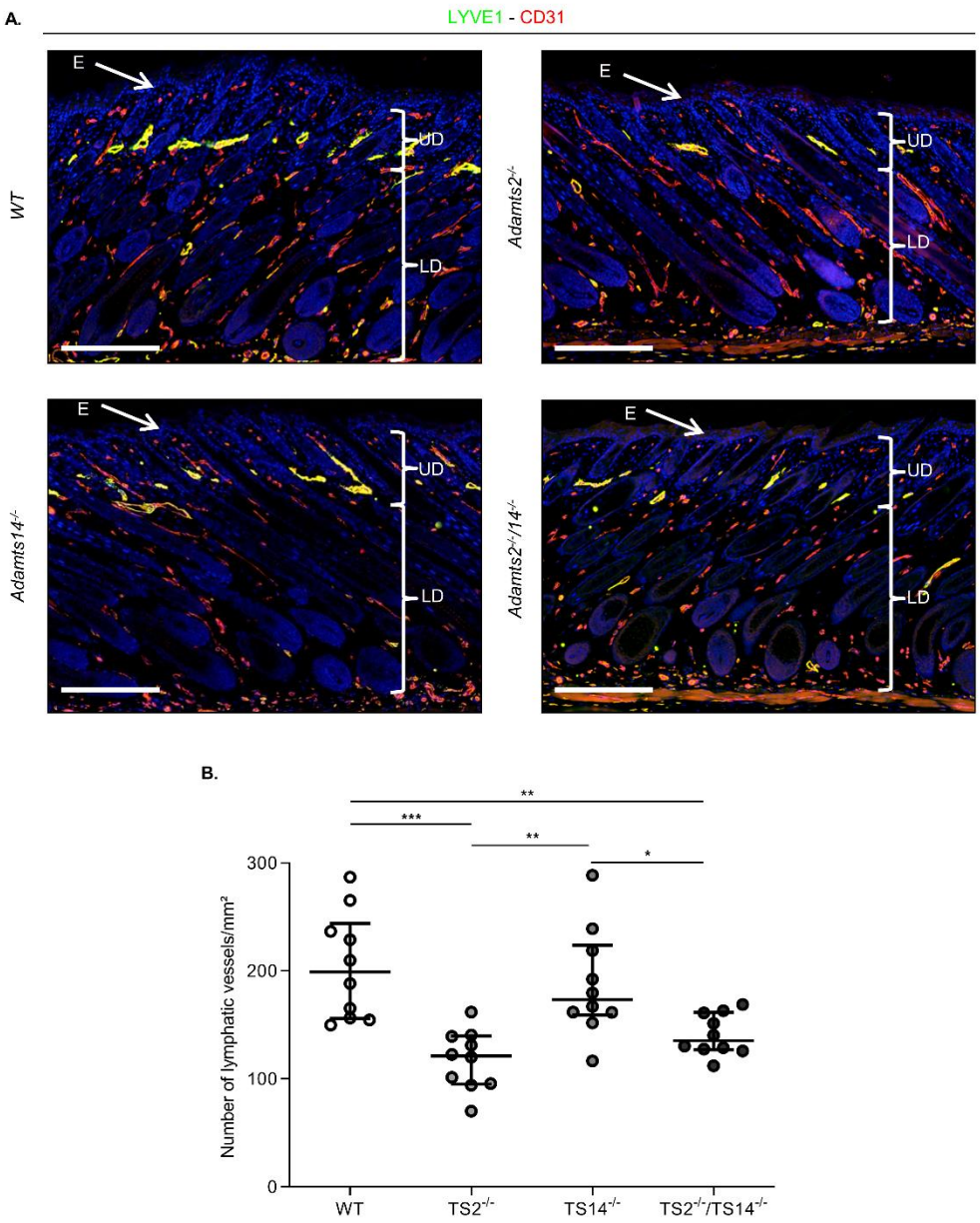

Figure 6: Absence of *Adamts2* affects lymphatic formation in postnatal (P6) mice.

Skin sections were stained using antibodies for LYVE1 (green) and CD31 (red) (scale bar: 200µm). A. Because of co-expression of LYVE1 and CD31, lymphatics appear as yellow structures, mainly in the upper dermis and in close association with the bulge region of the hair follicle (18). LYVE1 positive cells identified in the lower dermis and in the adipose tissue were mainly macrophages (Supplemental Figure 6). B. Computerized quantification of LYVE1 staining in the upper dermis. As compared to WT mice, less lymphatics were observed in $TS2^{-/-}$ and $TS2^{-/-}TS14^{-/-}$ mice. E: epidermis, UD: upper dermis, LD: lower dermis. Statistical analyses were performed using Kruskal-Wallis test followed by Holm-Sidak post hoc test for multiple comparisons. $*P < 0.05$; $**P < 0.01$; $***P < 0.001$.

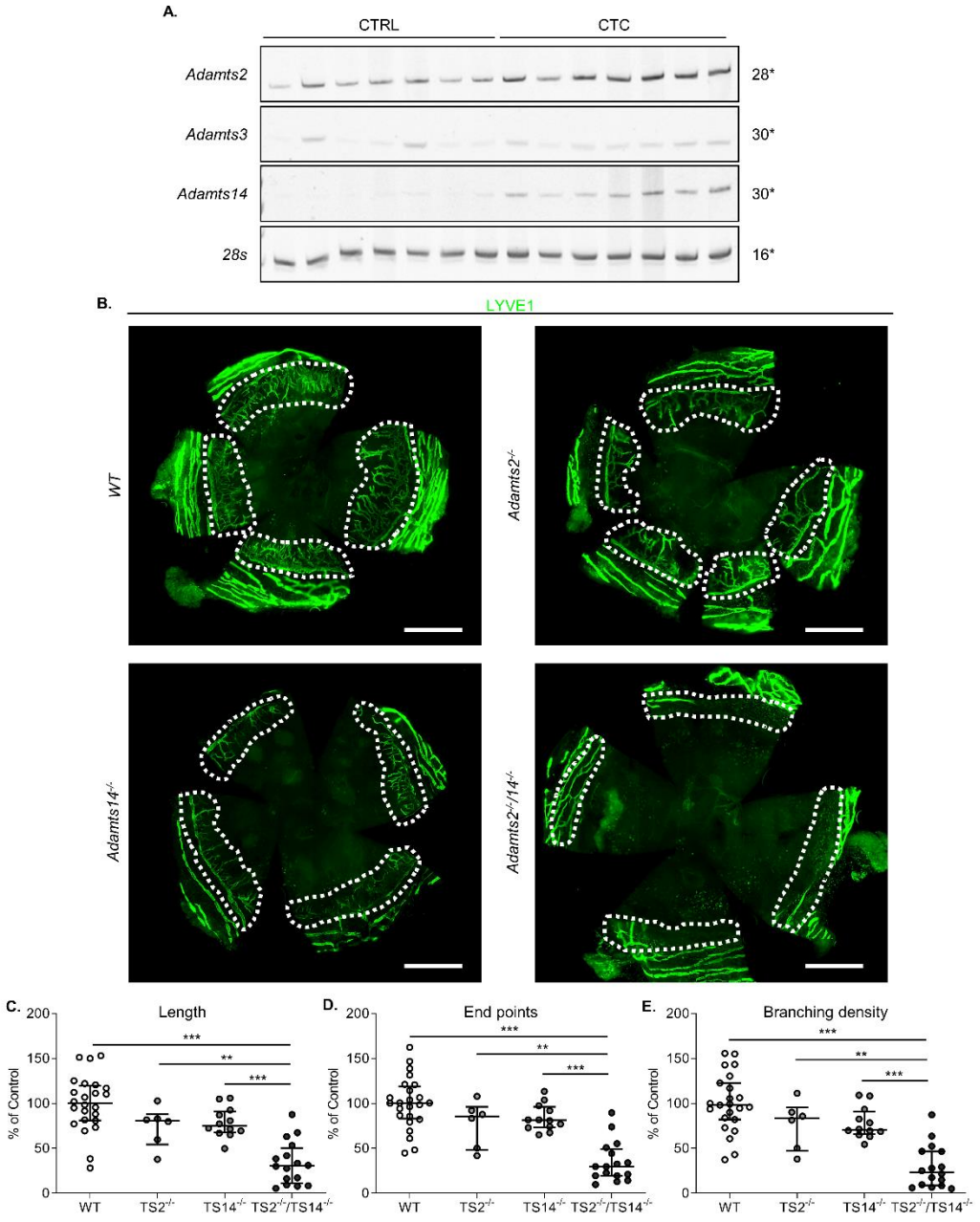

Figure 7: Absence of *Adamts2* or *Adamts14* inhibits inflammatory corneal lymphangiogenesis. A. Expression of *Adamts2* (28 cycles), *Adamts3* (30 cycles), *Adamts14* (30 cycles) and *28s* (as control, 16 cycles) by RT-PCR on cornea collected from uninjured (CTRL) WT mice (n=7) or from WT mice 7 days after corneal thermal cauterization (CTC) (n=7). The expressions of *Adamts2* and *Adamts14*, but not of *Adamts3*, were increased during the healing process of the injured cornea. B. Lymphatic vessels visualization using LYVE1 immunofluorescence on whole-mount cornea 7 days after thermal cauterization in WT, TS2$^{-/-}$, TS14$^{-/-}$ and TS2$^{-/-}$TS14$^{-/-}$ mice (scale bar: 1mm). A decrease of lymphatic vessels invading the injured cornea (white dotted lines) were observed in knockout mice as compared to WT mice. Computerized quantification of the length (C), end point numbers (D) and branching density (E) of lymphatic vessels in cornea 7 days after thermal cauterization in WT, TS2$^{-/-}$, TS14$^{-/-}$ and TS2$^{-/-}$TS14$^{-/-}$ mice expressed as percentage of WT control (n= 23 WT, 6 TS2$^{-/-}$, 12 TS14$^{-/-}$ and 16 TS2$^{-/-}$TS14$^{-/-}$ cornea). Statistical analyses were performed using Kruskal-Wallis test followed by Holm-Sidak post hoc test for multiple comparisons. $^{**}P < 0.01$; $^{***}P < 0.001$.